Molecular Recognition of the Substrate Diphosphate Group Governs Product Diversity in Trichodiene Synthase Mutants[†,‡]

L. Sangeetha Vedula,[§] Michael J. Rynkiewicz,[§,||] Hyung-Jung Pyun,[⊥,#] Robert M. Coates,[⊥] David E. Cane,[¶] and David W. Christianson*[,§]

Roy and Diana Vagelos Laboratories, Department of Chemistry, University of Pennsylvania, Philadelphia, Pennsylvania 19104-6323, Department of Chemistry, University of Illinois, Urbana, Illinois 61801, and Department of Chemistry, Brown University, Providence, Rhode Island 02912-9108

Received January 11, 2005; Revised Manuscript Received February 28, 2005

ABSTRACT: The X-ray crystal structures of Y305F trichodiene synthase and its complex with coproduct inorganic pyrophosphate (PP_i) and of Y305F and D100E trichodiene synthases in ternary complexes with PP_i and aza analogues of the bisabolyl carbocation intermediate are reported. The Y305F substitution in the basic D^{302}RRYR motif does not cause large changes in the overall structure in comparison with the wild-type enzyme in either the uncomplexed enzyme or its complex with PP_i. However, the loss of the Y305F−PP_i hydrogen bond appears to be compensated by a very slight shift in the position of the side chain of R304. The putative bisabolyl carbocation mimic, *R*-azabisabolene, binds in a conformation and orientation that does not appear to mimic that of the actual carbocation intermediate, suggesting that the avid inhibition by *R*- and *S*-azabisabolenes arises more from favorable electrostatic interactions with PP_i rather than any special resemblance to a reaction intermediate. Greater enclosed active-site volumes result from the Y305F and D100E mutations that appear to confer greater variability in ligand-binding conformations and orientations, which results in the formation of aberrant cyclization products. Because the binding conformations and orientations of *R*-azabisabolene to Y305F and D100E trichodiene synthases do not correspond to binding conformations required for product formation and because the binding conformations and orientations of diverse substrate and carbocation analogues to other cyclases such as 5-epi-aristolochene synthase and bornyl diphosphate synthase generally do not correspond to catalytically productive complexes, we conclude that the formation of transient carbocation intermediates in terpene cyclization reactions is generally under kinetic rather than thermodynamic control.

Terpenoids comprise one of the single largest families of natural products that serve a wide variety of biological functions in living systems (*1*, *2*). For instance, the diterpene (C_{20}) retinal plays a key role in vision (*2*); the triterpene (C_{30}) lanosterol is a precursor of cholesterol (*2*), which modulates the properties of biological membranes (*3*, *4*); and various bacteria and fungi produce sesquiterpenes (C_{15}) that exhibit potent antibacterial or antifungal properties (*2*). Notably, all terpenoids are ultimately derived from linear combinations of the simple isoprenoid (C_5) building block, isopentenyl diphosphate. Diverse cyclic terpenoids can be generated from isoprenoid precursors in cationic cyclization reactions catalyzed by terpenoid synthases, also called terpenoid cyclases (*5*−*9*). For example, sesquiterpenes derive from the acyclic precursor (*E*,*E*)-farnesyl diphosphate (FPP)[1] in a reaction catalyzed by a sesquiterpene cyclase. Each sesquiterpene cyclase serves as a template to hold FPP in the productive conformation for carbocation formation and cyclization, usually with high geometric and stereochemical precision. Some wild-type cyclases exhibit more relaxed control, however, and generate multiple products (*10*−*15*).

Amino acid substitutions in the active sites of highly precise terpenoid cyclases generally yield mutant cyclases that generate multiple products. For example, monoterpene, sesquiterpene, and diterpene cyclases contain the aspartate-rich motif DDXX(D,E) that binds catalytically obligatory Mg^{2+} (or sometimes Mn^{2+}) ions (*16*, *17*). This motif appears as D^{100}DSKD in trichodiene synthase, a dimeric sesquiterpene cyclase from *Fusarium sporotrichiodes* that cyclizes FPP to form the sesquiterpene hydrocarbon trichodiene (*18*, *19*) (Figure 1a). The seemingly conservative D100E mutation results in a 2.6-fold decrease in overall k_{cat} and a 22-fold

[†] This work was supported by National Institutes of Health Grants GM56838 (to D.W.C.), GM30301 (to D.E.C.), and GM13956 (to R.M.C.).

[‡] Atomic coordinates of trichodiene synthase mutants have been deposited in the Protein Data Bank with accession codes as follows: Y305F, 1YJ4; Y305F-Mg^{2+}_3-PP_i complex, 1YYQ; Y305F-Mg^{2+}_3-PP_i-*R*-azabisabolene complex, 1YYR; Y305F-Mg^{2+}_3-PP_i-*S*-azabisabolene complex, 1YYS; D100E-Mg^{2+}_2-PP_i-*R*-azabisabolene complex, 1YYT; and D100E-Mg^{2+}_2-PP_i-*S*-azabisabolene complex, 1YYU.

* To whom correspondence should be addressed: Roy and Diana Vagelos Laboratories, Department of Chemistry, University of Pennsylvania, 231 South 34th St., Philadelphia, PA 19104-6323. Telephone: 215-898-5714. Fax: 215-573-2201. E-mail: chris@xtal.chem.upenn.edu.

[§] University of Pennsylvania.

[||] Current address: Daiichi Asubio Medical Research Laboratories, LLC, One Kendall Square, Bldg. 700, Cambridge, MA 02139.

[⊥] University of Illinois.

[#] Current address: Gilead Sciences, 333 Lakeside Drive, Foster City, CA 94404.

[¶] Brown University.

[1] Abbreviations: FPP, (*E*,*E*)-farnesyl diphosphate; NPP, (3*R*)-nerolidyl diphosphate; PP_i, inorganic pyrophosphate; rms, root-mean-square.

10.1021/bi050059o CCC: $30.25
Published on Web 03/31/2005

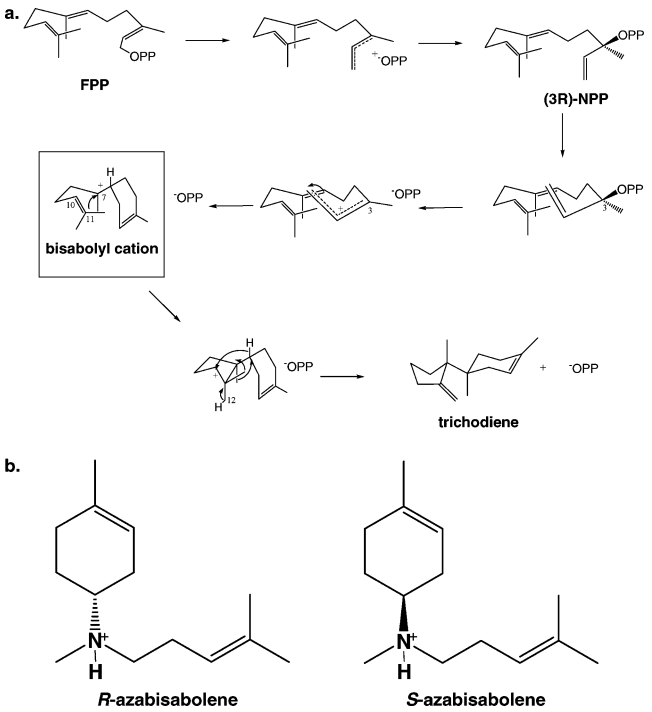

FIGURE 1: (a) Postulated mechanism for the cyclization of FPP to trichodiene by trichodiene synthase; OPP = diphosphate, NPP = nerolidyl diphosphate (*19*). Selected carbon atoms of substrate and intermediates are labeled. (b) *R*-Azabisabolene, a cationic analogue of the bisabolyl cation in the trichodiene synthase mechanism, is a strong competitive inhibitor in the presence of PP_i with $K_i = 0.51$ μM (*25*); similarly, the enantiomer *S*-azabisabolene binds in the presence of PP_i with $K_i = 0.47$ μM (*25*), suggesting that the stereochemical discrimination is weak at the corresponding step in catalysis.

decrease in k_{cat}/K_m as well as the generation of five aberrant sesquiterpene products in addition to trichodiene (Figure 2) (*20*). The additional products result from derailment and premature quenching of the normal carbocationic intermediates of the cyclization cascade. Therefore, Mg^{2+} binding is implicated in the stabilization of the active-site template with the proper conformation for FPP cyclization. The X-ray crystal structure of wild-type trichodiene synthase complexed with coproduct inorganic pyrophosphate (PP_i) and 3 Mg^{2+} ions reveals how Mg^{2+} binding is linked to template stabilization: the PP_i-$Mg^{2+}{}_3$ cluster induces a conformational change that completely sequesters the active site from the bulk solvent (*21*). In D100E trichodiene synthase, however, this PP_i-triggered conformational change is highly attenuated, resulting in an active-site cavity that is 12% greater in volume (*22*). Presuming that the diphosphate group of FPP similarly triggers active-site closure, the larger active-site cavity of D100E trichodiene synthase would permit additional conformational freedom for the substrate and reactive carbocation intermediates, thereby allowing for additional cyclization pathways. Accordingly, the molecular recognition of the substrate diphosphate group by metal coordination and hydrogen bonding plays a critical role in triggering conformational changes that stabilize the active-site template in the proper conformation for catalysis.

Metal coordination interactions appear to dominate the molecular recognition of diphosphate: PP_i, the aspartate-rich motif, and a second metal-binding motif (the "NSE loop") bind 3 Mg^{2+} ions in wild-type trichodiene synthase (*21*) and 2 Mg^{2+} ions in the D100E trichodiene synthase (*22*). However, trichodiene synthase also utilizes hydrogen bonds with R182, K232, R304, and Y305 to stabilize PP_i binding (*21*, *22*). The loss of the Y305-diphosphate hydrogen bond in Y305F trichodiene synthase has little effect on k_{cat} but increases K_m by a factor of 7−8; 25% of an aberrant product, α-cuprenene, is also generated (Figure 2) (*23*, *24*). The Y305T substitution has even more dramatic consequences, resulting in a 65-fold increase in K_m, a 160-fold decrease in k_{cat}, and a 4:4:4:1 product mixture of trichodiene, isochamigrene, and α- and *β*-bisabolenes, respectively (*24*).

To probe the relationship between diphosphate[2] recognition and catalysis by trichodiene synthase, we now focus on structural studies of two site-specific mutants: D100E, in which diphosphate−Mg^{2+} coordination interactions are perturbed, and Y305F, in which a single diphosphate hydrogen bond is perturbed. To ascertain mechanistic inferences on the binding of a cationic intermediate in catalysis by these mutants, we report the structures of D100E and Y305F trichodiene synthases complexed with (4*R*)-7-azabisabolene (designated "*R*-azabisabolene"), a cationic analogue of the normal bisabolyl carbocation intermediate, and its enantiomer (4*S*)-7-azabisabolene (designated "*S*-azabisabolene") (Figure 1b) (*25*).

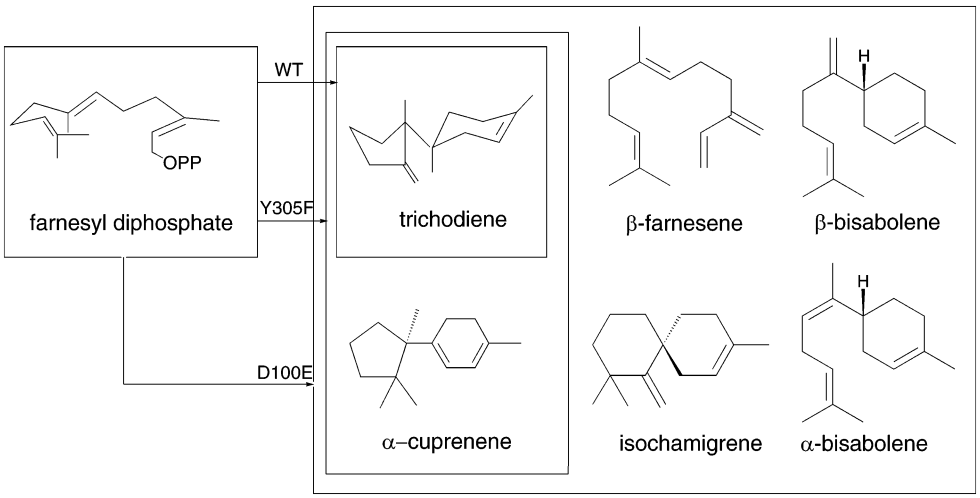

FIGURE 2: Cyclization of FPP catalyzed by wild-type (WT), Y305F, and D100E trichodiene synthases yields an increasingly diverse product array of linear and cyclic sesquiterpenes (OPP = diphosphate).

Table 1: Data Collection and Refinement Statistics

mutant/complex	Y305F	Y305F-$Mg^{2+}{}_3$-PP_i	Y305F-$Mg^{2+}{}_3$-PP_i -*R*-azabisabolene	Y305F-$Mg^{2+}{}_3$-PP_i -*S*-azabisabolene	D100E-$Mg^{2+}{}_2$-PP_i -*R*-azabisabolene	D100E-$Mg^{2+}{}_2$-PP_i -*S*-azabisabolene
resolution range (Å)	40−2.3	50−2.1	50−2.5	75−2.75	14−2.8	50−2.95
reflections (measured/unique)	162 490/54 949	378 002/75 643	233 822/45 564	166 950/33 388	115 571/31 744	128 454/27 593
completeness (%) (overall/outer shell)	93.9/94.6	99.4/100	99/91	99.8/100.0	97.2/93.6	97.6/97.0
R_{merge}[a] (overall/outer shell)	0.059/0.448	0.086/0.424	0.126/0.409	0.104/0.494	0.098/0.393	0.093/0.412
$\langle I/\sigma \rangle$ (overall/outer shell)	22/3.1	16/3.4	13.2/2.2	19.3/2.9	16.7/3.0	21.4/3.0
protein atoms (number)[b]	5753	5802	5802	5795	5816	5788
solvent atoms (number)[b]	175	207	54	30	71	93
metal ions (number)[b]	0	3	3	3	2	4
ligand atoms (number)[b]	0	9	39	24	39	48
reflections used in refinement (work/free)	52 054/2770	71 575/3829	42 759/2263	31 694/1657	24 979/2010	26 029/1342
R/R_{free}[c]	0.244/0.275	0.239/0.261	0.219/0.256	0.248/0.274	0.225/0.269	0.218/0.254
rms deviations						
bonds (Å)	0.007	0.006	0.007	0.007	0.008	0.007
angles (deg)	1.1	1.1	1.2	1.2	1.2	1.2
dihedral angles (deg)	18.5	18.4	18.7	18.7	18.6	18.0
improper dihedral angles (deg)	0.8	0.7	0.8	0.8	0.8	0.8

[a] $R_{merge} = \sum|I_j - \langle I_j \rangle|/\sum I_j$, where I_j is the observed intensity for reflection j and $\langle I_j \rangle$ is the average intensity calculated for reflection j from replicate data. [b] Per asymmetric unit. [c] $R = \sum||F_o| - |F_c||/\sum|F_o|$, where R and R_{free} are calculated by using the working and test reflection sets, respectively.

MATERIALS AND METHODS

Mutants of trichodiene synthase from *F. sporotrichioides* were prepared, overexpressed in *Escherichia coli*, purified as described (*21*, *26*), and crystallized by the hanging drop vapor diffusion method described for wild-type and D100E trichodiene synthases (*21*, *22*). Crystals of Y305F trichodiene synthase were soaked in PP_i buffers using the same protocol employed for the preparation of PP_i complexes with wild-type and D100E trichodiene synthases (*21*, *22*). The complexes with *S*-azabisabolene were prepared by soaking mutant enzyme crystals overnight in a buffer solution containing 1 mM $MgCl_2$, 2 mM $Na_4P_2O_7$ (pH 6.9), and 3 mM *S*-azabisabolene. The complex between D100E trichodiene synthase and *R*-azabisabolene was prepared by cocrystallizing the enzyme with 5 mM $MgCl_2$, 1 mM $Na_4P_2O_7$ (pH 6.9), and 0.5 mM *R*-azabisabolene; immediately after harvest, crystals were further soaked overnight in a buffer solution containing 1 mM $MgCl_2$, 10 mM $Na_4P_2O_7$ (pH 6.9), and 1 mM *R*-azabisabolene. The complex between Y305F trichodiene synthase and *R*-azabisabolene was prepared by soaking crystals of the enzyme overnight in a buffer solution containing 1 mM $MgCl_2$, 2 mM $Na_4P_2O_7$ (pH 6.9), and 3 mM *R*-azabisabolene. Each mutant and/or complex crystallized essentially isomorphously with the wild-type enzyme (space group = $P3_121$, $a = b = 122.2$ Å, $c = 151.2$ Å) (*21*). Crystals were prepared for data collection by cryoprotection in 25% ethylene glycol and flash-cooling in liquid nitrogen. Although we were able to prepare crystals of wild-type trichodiene synthase complexed with $Mg^{2+}{}_3$-PP_i and *R*-azabisabolene, these crystals suffered from excessive mosaicity and did not yield useable X-ray diffraction data.

Diffraction data from crystals of the D100E trichodiene synthase-$Mg^{2+}{}_2$-PP_i-*R*-azabisabolene complex were collected on an R-AXIS IIc image plate area detector using copper rotating anode Cu−K_α radiation. Diffraction data from crystals of unliganded Y305F trichodiene synthase were collected at the Brookhaven National Laboratory (beamline X4A, $\lambda = 1.0721$ Å). Diffraction data from crystals of the Y305F trichodiene synthase-$Mg^{2+}{}_3$-PP_i complex were collected at the Brookhaven National Laboratory (beamline X12C, $\lambda = 1.100\,04$ Å). Diffraction data from crystals of the Y305F trichodiene synthase-$Mg^{2+}{}_3$-PP_i-*R*-azabisabolene complex were collected at Advanced Light Source, Berkeley, CA (beamline BL 5.0.2, $\lambda = 1.000\,00$ Å). Diffraction data from crystals of the Y305F trichodiene synthase-$Mg^{2+}{}_3$-PP_i-*S*-azabisabolene and D100E trichodiene synthase-$Mg^{2+}{}_2$-PP_i-*S*-azabisabolene complexes were collected at the Cornell High Energy Synchrotron Source (beamline A1, $\lambda = 0.9764$ Å). Data were indexed and merged using HKL2000 (*27*). The structures were solved by the difference Fourier technique. CNS (*28*) and O (*29*) were used in refinement and rebuilding, respectively. Noncrystallographic symmetry constraints were used in the initial stages of refinement and subsequently relaxed into appropriately weighted restraints as judged by R_{free} as refinement progressed. In each structure, disordered loops characterized by poor electron density were not included in the final model. Electron-density maps and molecular models shown in the figures were prepared with Bobscript, version 2.4 (*30*, *31*). Data collection and refinement statistics are reported in Table 1.

[2] Because the PP_i product and the FPP diphosphate group are likely to make identical metal coordination interactions in the enzyme active site, the term "diphosphate" is used as a generic designation of either FPP or PP_i.

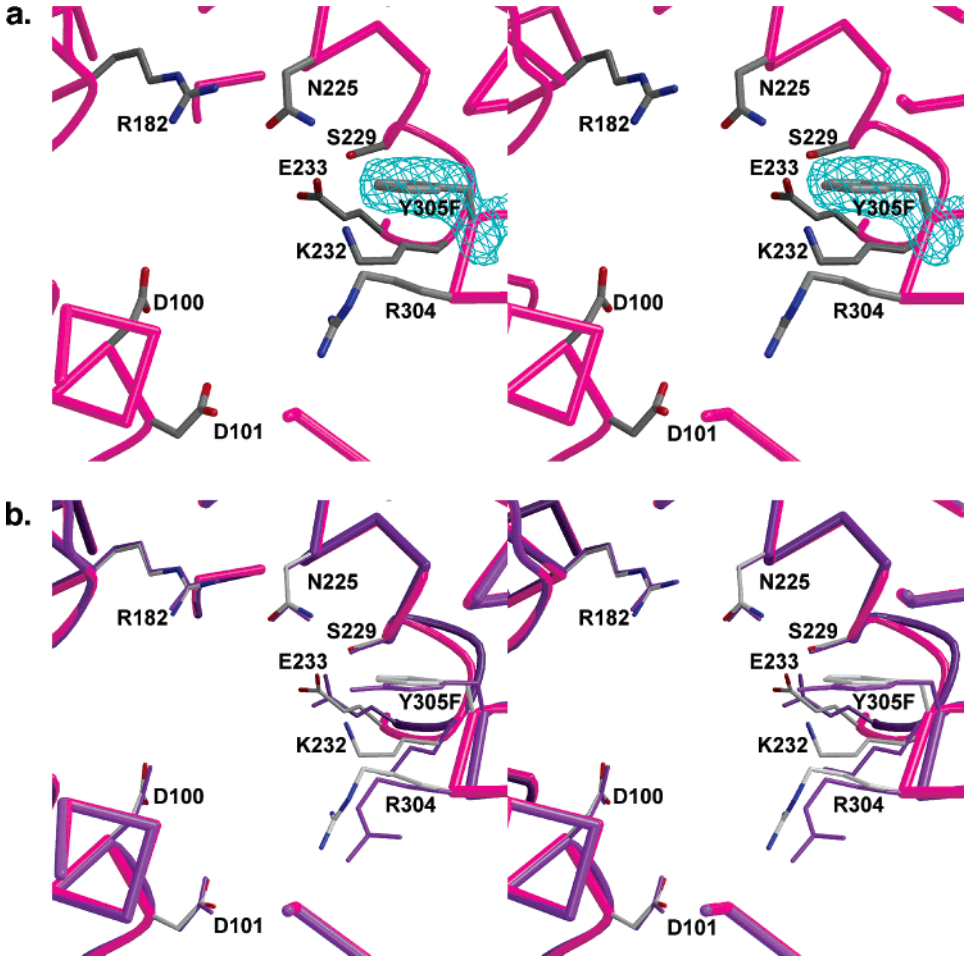

FIGURE 3: Active site of uncomplexed Y305F trichodiene synthase. (a) Simulated annealing omit map of F305 contoured at 4.0σ. The mutated side chain is well-defined by clear electron density. (b) Superposition of the active sites of the uncomplexed wild-type (purple) and Y305F (magenta) trichodiene synthases.

RESULTS

Y305F Trichodiene Synthase. The structure of Y305F trichodiene synthase is identical to that of the wild-type enzyme (*21*) with a few local variations in the active site (Figure 3). The root-mean-square (rms) deviation between the two structures is 0.41 Å for 354 C_α atoms. The uncomplexed enzyme does not bind metal ions, indicating that diphosphate binding is required for high-affinity metal recognition.

Y305F Trichodiene Synthase-$Mg^{2+}{}_3$-PP_i Complex. The $Mg^{2+}{}_3$-PP_i cluster binds to the active site of monomer B of the dimer (Figure 4). Because the polypeptide segments that must undergo diphosphate-induced conformational changes in monomer A make interlattice crystal contacts, there is a barrier for $Mg^{2+}{}_3$-PP_i binding to this monomer, as noted for crystals of the wild-type enzyme (*21*). As for the wild-type enzyme (*21*), PP_i binding triggers conformational changes of D101 and R304 so that they form a salt link and cap the active-site cavity. The rms deviation between the unliganded and liganded forms of the Y305F mutant is 1.4 Å for 351 C_α atoms. The most significant deviations found are for polypeptide segments that interact with $Mg^{2+}{}_3$-PP_i: M1-E31, T96-E133, Y231−I241, and C301−W343. These conformational changes are, in general, similar to the diphosphate-induced conformational changes described for the wild-type enzyme (*21*). Metal ions bound in the active site are coordinated by D100, N225, S229, E233, and PP_i (Figure 4). The PP_i anion is stabilized by metal ion coordination interactions and hydrogen bonds with R182, R304, and K232. In wild-type and D100E trichodiene synthases, the PP_i anion also receives a hydrogen bond from Y305 (*21*, *22*). The loss of this hydrogen bond in the Y305F mutant may be compensated by a very slight shift in the position of the side chain of R304, which forms a second hydrogen bond with PP_i (Figure 4).

Y305F Trichodiene Synthase-$Mg^{2+}{}_3$-PP_i- R-Azabisabolene Complex. The $Mg^{2+}{}_3$-PP_i-*R*-azabisabolene cluster binds to the active site of monomer B of the trichodiene synthase dimer (Figure 5), while *R*-azabisabolene alone binds in the active site of monomer A. The rms deviation between the $Mg^{2+}{}_3$-PP_i-bound and $Mg^{2+}{}_3$-PP_i-*R*-azabisabolene-bound Y305F trichodiene synthase structures is 0.17 Å for 351 C_α atoms. Metal ions are coordinated by D100, N225, S229, E233, and PP_i. The PP_i anion is stabilized by metal-coordination interactions and hydrogen bonds with R182, K232, and R304 (Figure 5).

The tertiary ammonium cation of *R*-azabisabolene was originally designed to mimic the bisabolyl carbocation intermediate (*25*), and binding is synergized by PP_i. In the crystal structure, although there are no hydrogen-bond interactions with the positively charged ammonium cation, it is presumably stabilized by long-range ionic interactions

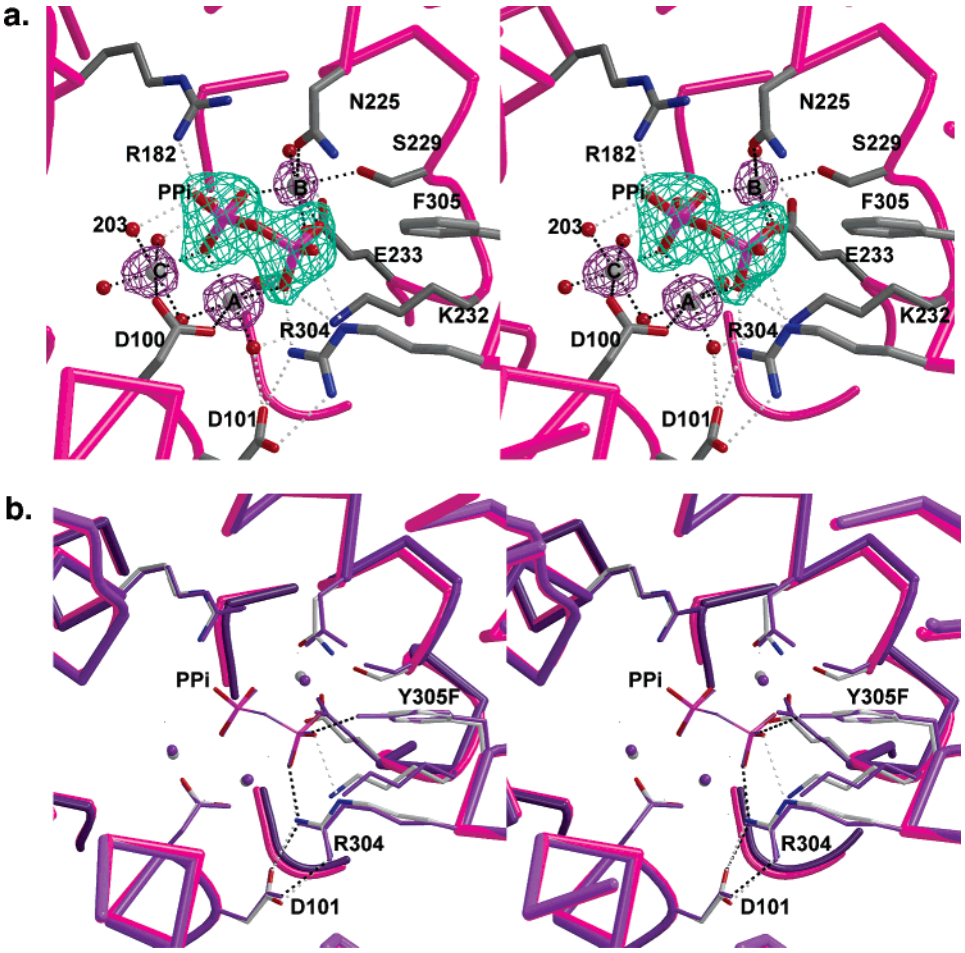

FIGURE 4: Active site of the Y305F trichodiene synthase-Mg^{2+}_3-PP_i complex. (a) Simulated annealing omit maps of PP_i and metal ions are cyan and maroon, respectively, contoured at 7.4σ. Gray spheres represent metal ions, and red spheres represent water molecules. Hydrogen-bonding and metal-coordination interactions are represented by white and black broken lines, respectively. For clarity, only metal-coordinated solvent molecules are shown. Water 203, which is sequestered in the active-site cavity and potentially exposed to bound substrate, is indicated. (b) Superposition of the active sites of PP_i-bound wild-type (purple) and Y305F (magenta) trichodiene synthases. Hydrogen bonds are represented by black broken lines for the wild-type enzyme and white broken lines for the Y305F mutant. Note that R304 of the Y305F mutant appears to move slightly closer to PP_i, possibly compensating for the lost hydrogen bond in the mutant. For clarity, water molecules are omitted.

because the closest PP_i oxygen atom is 3.6 Å away from the ammonium nitrogen atom of the aza analogue. Given that *R*-azabisabolene facilitates the binding of PP_i in the absence of metal ions (unpublished results), we presume that the *R*-azabisabolene is indeed bound as the ammonium cation and that its electrostatic interactions with PP_i are favorable.

Y305F-Mg^{2+}_3-PP_i-S-Azabisabolene Complex. Surprisingly, the Mg^{2+}_3-PP_i cluster alone binds in the active site of monomer B, while *S*-azabisabolene alone binds in the active site of monomer A (Figure 6) of the trichodiene synthase dimer. The active site of monomer B contains additional uninterpretable density that might indicate the binding of disordered and/or partial-occupancy *S*-azabisabolene. It is possible that the binding of the *S*-stereoisomer of azabisabolene is disfavored for this mutant. Monomer B undergoes the characteristic diphosphate-induced conformational change that caps the active site, whereas the active site of monomer A remains open. The rms deviation between 349 C_α atoms of monomers A and B is 1.3 Å. Metal and PP_i interactions in monomer B are similar to those observed in the Y305F trichodiene synthase-Mg^{2+}_3-PP_i complex.

D100E-Mg^{2+}_2-PP_i-R-Azabisabolene Complex. The Mg^{2+}_2-PP_i-*R*-azabisabolene cluster binds only in the active site of monomer B of the D100E trichodiene synthase dimer (Figure 7) and the diphosphate-induced active-site closure is highly attenuated, consistent with the D100E trichodiene synthase-Mg^{2+}_2-PP_i complex (*22*). *R*-Azabisabolene alone binds in the active site of monomer A. The rms deviation between the Mg^{2+}_2-PP_i-bound and Mg^{2+}_2-PP_i-*R*-azabisabolene-bound D100E trichodiene synthase structures is 0.54 Å for 354 C_α atoms. The metal ions, Mg^{2+}_A and Mg^{2+}_B, that bind in the active site of this complex, appear to be stabilized only by long-range (2.6−3.2 Å) interactions with PP_i, N225, S229, and E233. This may be a consequence of the moderate resolution of the structure determination. However, it may also be a consequence of a noticeable change in PP_i binding that results in perturbed metal-coordination interactions (Figure 7b).

Although there are no hydrogen-bond interactions with the positively charged ammonium cation of *R*-azabisabolene, it is presumably stabilized by long-range ionic interactions because the closest PP_i oxygen atom is 3.8 Å away from the ammonium nitrogen atom of the inhibitor.

D100E Trichodiene Synthase-Mg^{2+}_2-PP_i-S-Azabisabolene Complex. The Mg^{2+}_2-PP_i-*S*-azabisabolene cluster binds in the active sites of monomers A and B of the D100E trichodiene

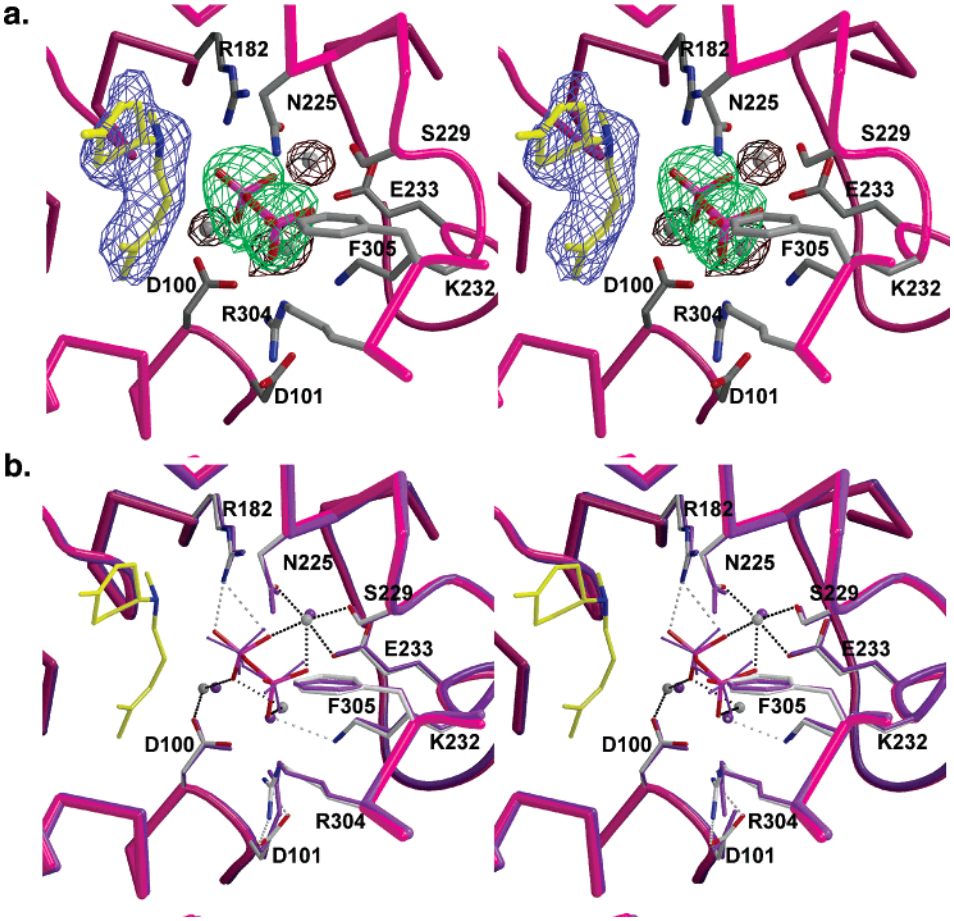

FIGURE 5: Active site of the Y305F trichodiene synthase-Mg^{2+}_3-PP_i-*R*-azabisabolene complex. (a) Simulated annealing omit maps of *R*-azabisabolene (blue, 6.0σ), PP_i (green, 7.6σ), and metal ions (maroon, 7.4σ). (b) Superposition with the Y305F trichodiene synthase-Mg^{2+}_3-PP_i complex (purple). For clarity, water molecules are omitted. Hydrogen-bond and metal-coordination interactions are represented by white and black broken lines, respectively.

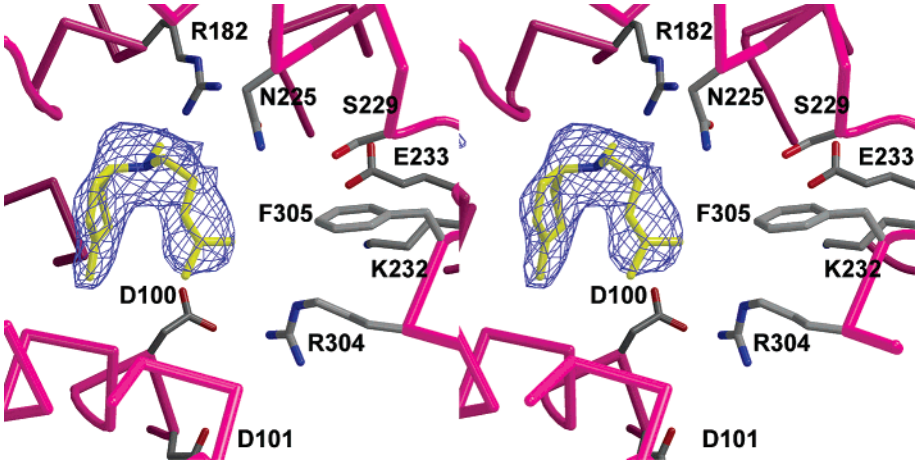

FIGURE 6: Simulated annealing omit map of *S*-azabisabolene (blue, 4.5σ) bound to the active site of monomer A of Y305F trichodiene synthase.

synthase dimer (Figure 8a). Interestingly, this is the only complex in which both active sites simultaneously bind PP_i and azabisabolene ligands. The diphosphate-induced active-site closure observed for wild-type trichodiene synthase (*21*) is highly attenuated in this structure, as also observed for the corresponding complex with *R*-azabisabolene (Figure 7) as well as the D100E trichodiene synthase-Mg^{2+}_2-PP_i complex (*22*). The rms deviation between the Mg^{2+}_2-PP_i-bound and Mg^{2+}_2-PP_i-*S*-azabisabolene-bound D100E trichodiene synthase structures is 0.50 Å for 354 C_α atoms (Figure 8b). Metal ion stoichiometry is similar to that observed in the D100E trichodiene synthase-Mg^{2+}_2-PP_i complex (*22*). The coordination interactions of PP_i with both metal ions lengthen to 2.7−2.9 Å and Mg^{2+}_B coordination by S229 lengthens to 2.8 Å, too long to be considered inner-sphere interactions (these changes could be due in part to the moderate resolution of the structure determination). The PP_i anion is stabilized by metal-coordination interactions and hydrogen-bond interactions with the side chains of R182, Y305, and R304. Interestingly, the position and orientation

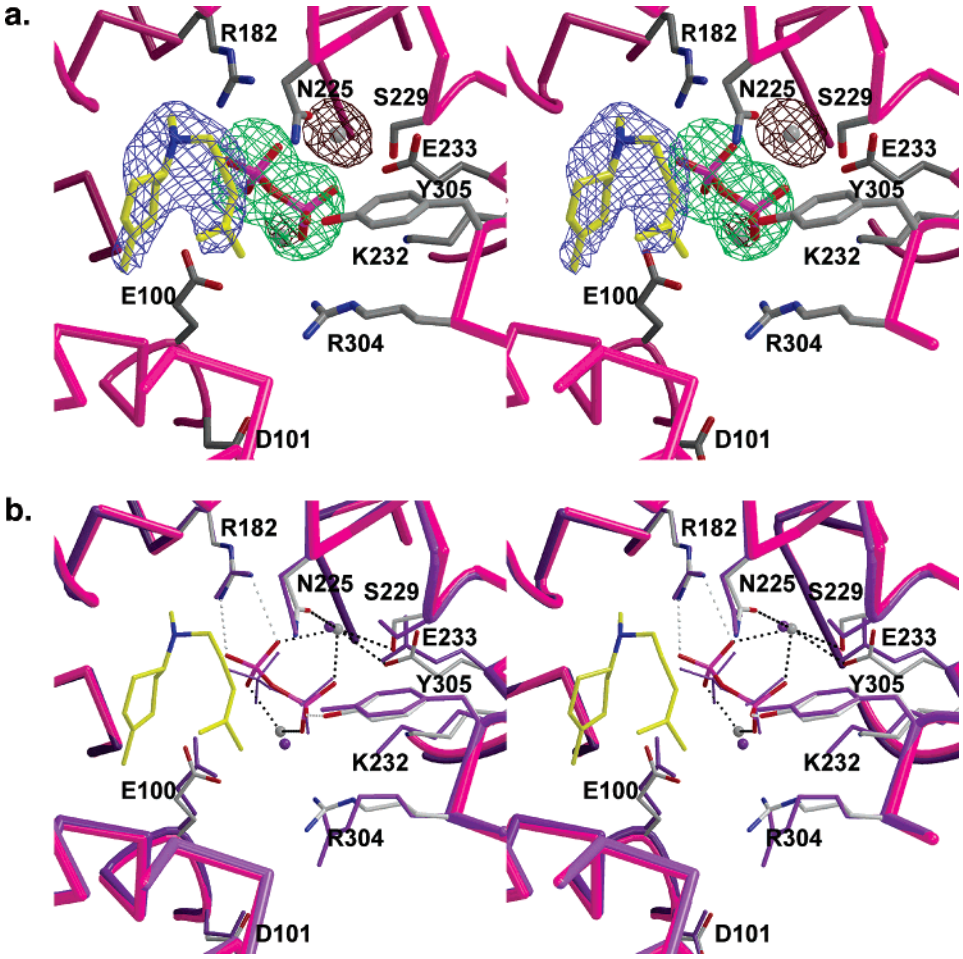

FIGURE 7: Active site of the D100E trichodiene synthase-Mg^{2+}_2-PP_i-*R*-azabisabolene complex. (a) Simulated annealing omit maps of R-azabisabolene (blue, 3.6σ), PP_i (green, 5.7σ), and metal ions (maroon, 4.2σ). (b) Superposition with the D100E trichodiene synthase-Mg^{2+}_2-PP_i complex (purple). Hydrogen-bond and metal-coordination interactions are represented by white and black broken lines, respectively.

of PP_i is noticeably different from that in the D100E trichodiene synthase complex with Mg^{2+}_2-PP_i (Figure 8b).

S-azabisabolene is the enantiomer of *R*-azabisabolene, the ammonium cation that was originally designed to mimic the configuration of the bisabolyl carbocation intermediate. Although there are no hydrogen-bond interactions with the positively charged ammonium cation, it is presumably stabilized by long-range ionic interactions because the closest PP_i oxygen atom is 4.2 Å away from the nitrogen atom of the aza analogue.

DISCUSSION

Trichodiene synthase protects highly reactive carbocation intermediates (Figure 1a) from being quenched prematurely by solvent or coproduct PP_i, while it stabilizes these intermediates by long-range electrostatic interactions, e.g., with PP_i, peptide backbone carbonyl groups, or the ring π electrons of aromatic residues in the active site. The PP_i anion has a slightly different position and orientation in the active sites of trichodiene synthase mutants complexed with the azabisabolenes in comparison to that observed in the respective mutants complexed only with metal ions and PP_i. Variations in PP_i binding are particularly evident in the structures of D100E trichodiene synthase complexes (Figures 7 and 8). This contrasts with the binding of PP_i to bornyl diphosphate synthase (a monoterpene cyclase), in which PP_i adopts a nearly uniform position and orientation regardless of whether substrate analogue, product, or aza analogue and PP_i are bound in the active site of the wild-type enzyme (*32*). Thus, if precise positional control of the substrate diphosphate group/PP_i product is required for effective catalysis, amino acid substitutions can degrade this control, either by holding PP_i fixed in a single, alternative orientation or by allowing multiple alternative orientations.

For Y305F trichodiene synthase, PP_i binding is identical to that observed in the wild-type enzyme apart from the loss of the Y305F−PP_i hydrogen bond (Figure 4); with *R*-azabisabolene bound in the active site, the PP_i position changes slightly (Figure 5; average PP_i atomic shift = 0.5 Å). For D100E trichodiene synthase, the orientation and position of PP_i binding and Mg^{2+} stoichiometry are significantly altered (*22*), and the binding of PP_i to this mutant is even further perturbed depending on whether *R*-azabisabolene or *S*-azabisabolene is bound in the active site (Figures 7 and 8, respectively). The average PP_i atomic shifts are 0.6 and 0.9 Å in the complexes with *R*- and *S*-azabisabolenes, respectively. These differences are greater than the rms coordinate error of 0.3−0.4 Å indicated by Luzzati plots, which typically overestimate experimental error. The significantly altered interaction with PP_i, resulting in a large part from weakened binding of Mg^{2+}_C, allows for alternative substrate and intermediate conformations that lead to the generation of a substantially broader product array by D100E trichodiene synthase (Figure 2).

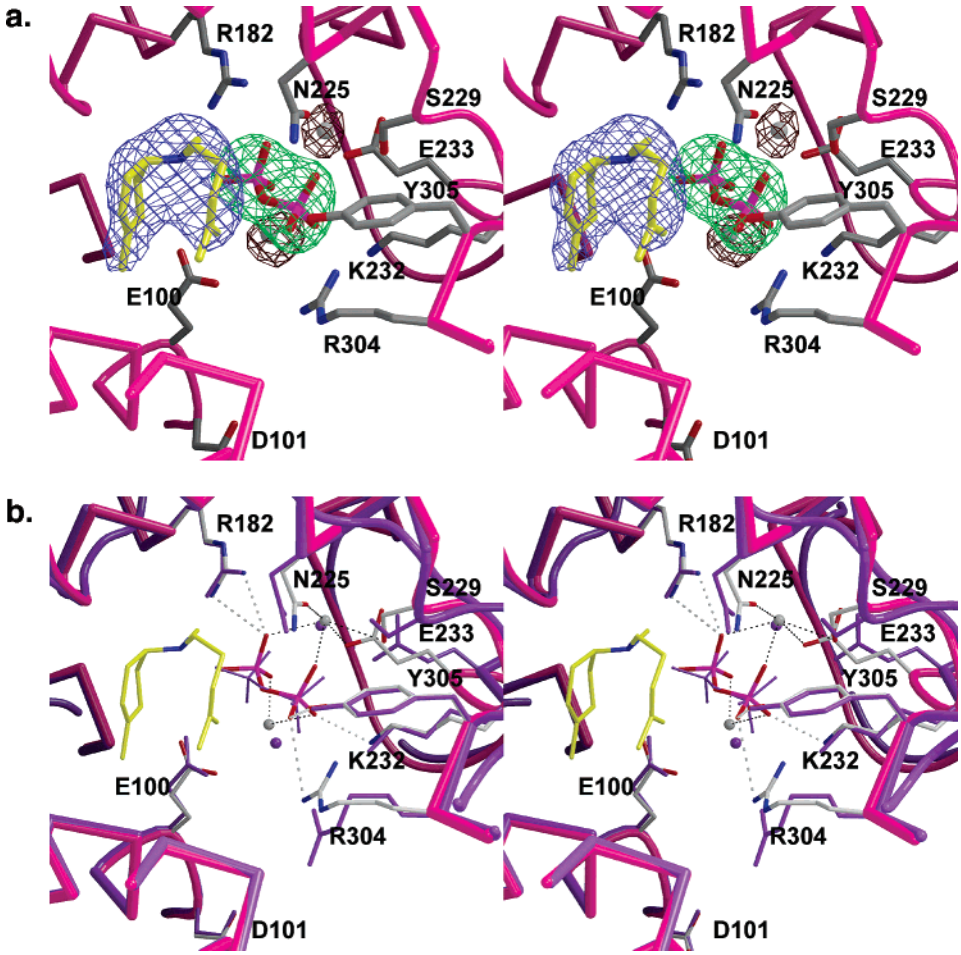

FIGURE 8: Active site of D100E trichodiene synthase-$Mg^{2+}{}_2$-PP_i-*S*-azabisabolene complex. (a) Simulated annealing omit maps of *S*-azabisabolene (blue, 5.3σ), PP_i (green, 7.2σ), and metal ions (maroon, 5.5σ). (b) Superposition with the D100E trichodiene synthase-$Mg^{2+}{}_2$-PP_i complex (purple). Hydrogen-bond and metal-coordination interactions are represented by white and black broken lines, respectively.

The presence of $Mg^{2+}{}_C$ in the active sites of ligand-bound Y305F and wild-type (*21*) trichodiene synthases allows coordination of water 203 (Figure 4), which forms part of the active-site template. The presence of water 203 contributes to the smaller enclosed active-site volumes of the wild-type and Y305F trichodiene synthases in comparison with D100E trichodiene synthase, which does not bind $Mg^{2+}{}_C$. It is notable that a water molecule contributes to the active-site contour of trichodiene synthase, just as a water molecule contributes to the active-site contour of bornyl diphosphate synthase, a monoterpene cyclase (*32*). In wild-type trichodiene synthase, water 203 is presumably hindered from reacting with the substrate by coordination to $Mg^{2+}{}_C$ and hydrogen-bond interactions with PP_i and the backbone carbonyl oxygen of N185.

A comparison of the active-site volumes of the wild-type and mutant trichodiene synthases indicates that, in general, a significantly greater enclosed active-site volume in PP_i complexes as calculated with the CastP server (*33*−*35*; http://cast.engr.uic.edu/cast) correlates with greater product diversity. For example, Y305F trichodiene synthase complexed with $Mg^{2+}{}_3$-PP_i exhibits only a slight decrease in the enclosed active-site volume, and the complex with $Mg^{2+}{}_3$-PP_i and *R*-azabisabolene exhibits a modest increase in the enclosed active-site volume (Table 2). This mutant generates a single aberrant product (25% α-cuprenene) in addition to trichodiene (*23*, *24*). In contrast, the complexes of D100E trichodiene synthase with $Mg^{2+}{}_2$-PP_i, with or without azabisabolene, reveal consistent ~15% increases in enclosed active-site volumes compared with the wild-type enzyme (Table 2). The chemical consequence of a greater active-site volume is less structural and stereochemical in precision of the cyclization cascade, and this results in the formation of significant quantities of five aberrant cyclization products (Figure 2) (*20*).

Table 2: Enclosed Active-Site Volumes in Trichodiene Synthase[a]

enzyme	ligand(s)	volume (Å^3)
wild type	$Mg^{2+}{}_3$-PP_i	437
Y305F	$Mg^{2+}{}_3$-PP_i	411
Y305F	$Mg^{2+}{}_3$-PP_i-*R*-azabisabolene	456
D100E	$Mg^{2+}{}_2$-PP_i	492
D100E	$Mg^{2+}{}_2$-PP_i-*R*-azabisabolene	513
D100E	$Mg^{2+}{}_2$-PP_i-*S*-azabisabolene	516

[a] Active-site volumes calculated using the CastP server http://cast.engr.uic.edu/cast (*33*−*35*). Note that the volumes reported here are different from those reported in ref *22*; this difference is due to the different algorithms used for volume calculation by CastP and VOIDOO.

In the trichodiene synthase mechanism, the nerolidyl diphosphate (NPP) intermediate re-ionizes to form a cisoid allylic carbocation that cyclizes to form the bisabolyl carbocation intermediate (Figure 1a). Presumably, the PP_i leaving group should remain reasonably close to C3, and C11 should be oriented for attack of the pro-*S* face of the

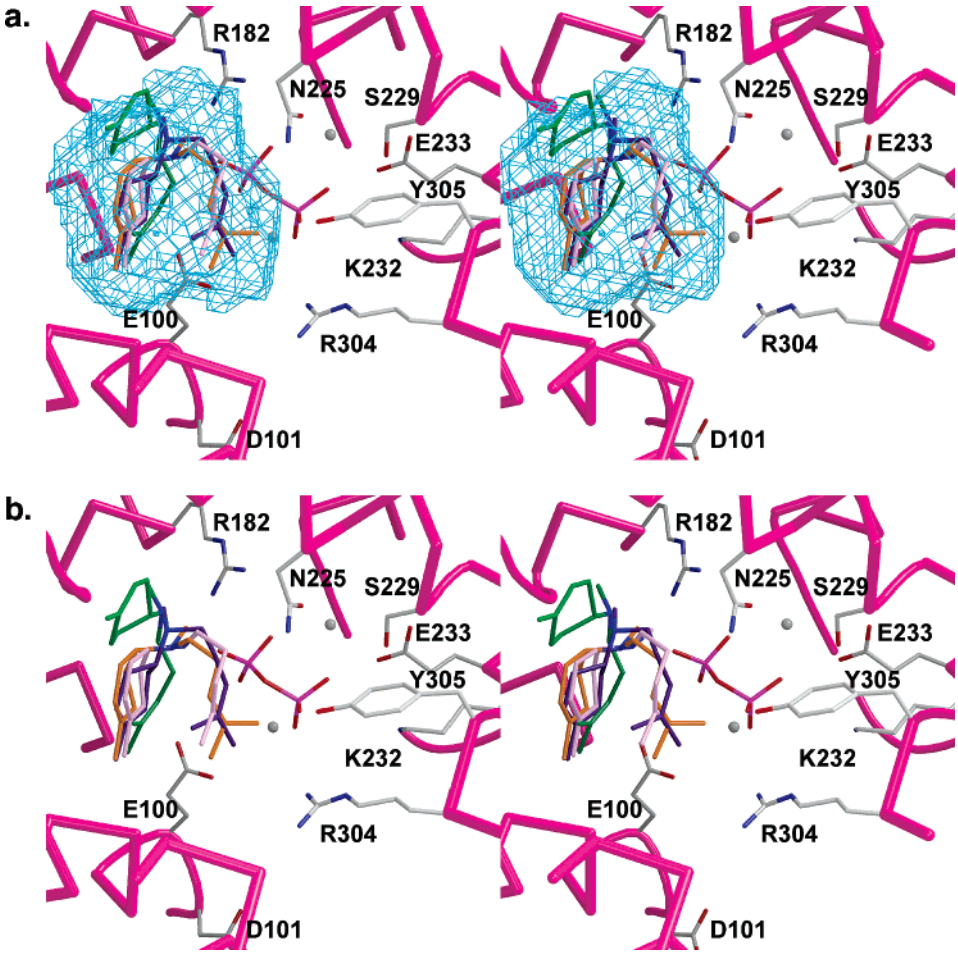

FIGURE 9: (a) Structure of the D100E trichodiene synthase-Mg^{2+}_2-PP_i complex superimposed on the experimental binding conformations of *R*-azabisabolene complexed with Y305F trichodiene synthase-Mg^{2+}_3-PP_i (green with blue nitrogen atom) and D100E trichodiene synthase-Mg^{2+}_2-PP_i (violet with blue nitrogen atom) and *S*-azabisabolene complexed with Y305F trichodiene synthase-Mg^{2+}_3-PP_i (orange with blue nitrogen atom) and D100E trichodiene synthase-Mg^{2+}_2-PP_i (pink with blue nitrogen atom). The accessible surface area of the active-site cavity is shown in cyan as calculated with VOIDOO (*39*, *40*). (b) Same as (a) but without the active-site surface contour, for clarity.

C7 carbocation. However, the putative mimic of the bisabolyl carbocation, *R*-azabisabolene, binds to Y305F and D100E trichodiene synthases such that the C3 atom of the analogue is positioned behind the positively charged ammonium cation relative to the PP_i group, rather than proximal to the PP_i, as it would be in the actual bisabolyl cation intermediate (even though *R*-azabisabolene binds with a different conformation and orientation to each mutant). Moreover, in the *R*-azabisabolene complex with Y305F trichodiene synthase, a more compact conformation of *R*-azabisabolene would result in an attack on the pro-*R* face of the C7 carbocation, which would ultimately result in the formation of the wrong diastereomer of trichodiene. Therefore, we conclude that *R*-azabisabolene binds to the active site of Y305F trichodiene synthase with a conformation that is inconsistent with the productive conformation of the bisabolyl carbocation generated in the course of the actual cyclization of FPP to trichodiene.

The apparent anomalous binding of *R*-azabisabolene may result from strong electrostatic interactions between the positively charged ammonium nitrogen atom and the negatively charged PP_i group, as was also concluded for the anomalous binding of the carbocation analogue 7-aza-7,8-dihydrolimonene to bornyl diphosphate synthase (*32*). Another factor possibly contributing to the anomalous binding mode may be the tetrahedral sp^3 geometry at the ammonium nitrogen of *R*-azabisabolene, which contrasts with the trigonal planar sp^2 configuration of the tertiary bisabolyl carbocation intermediate that it is intended to mimic.

If the nonproductive binding conformations and orientations observed in terpene cyclase complexes with cationic aza analogues are sterically accessible to actual carbocation intermediates, then it is notable that the corresponding aberrant products, such as an alternative diastereomer of trichodiene, are never formed by the wild-type enzyme. It is likely, however, that the bound conformation of the enzymatically generated bisabolyl cation reflects that of the NPP precursor from which it is formed and that this bisabolyl cation intermediate does not reorient significantly prior to further cyclization. The conformation and orientation of the enzymatically generated bisabolyl cation intermediate are therefore under kinetic control rather than thermodynamic control. Indeed, the positioning of the carbocation center remote from the PP_i counterion, with the cyclohexene ring interposed between the two charged species, may actually contribute to the driving force for further cyclization. Pre-steady-state kinetic studies (*36*) show that the ionization of the FPP in the active site is the slowest chemical step, with a first-order rate constant of 4 s^{-1} at 15 °C, while cyclization of NPP to trichodiene has a net rate constant of 200 s^{-1}.

The latter rate almost certainly precludes major reorientation of the bisabolyl cation intermediate within the active-site cavity in the course of the normal cyclization reaction.

It is notable that the active site of the D100E trichodiene synthase-Mg^{2+}_2-PP_i-*R*-azabisabolene complex is sufficiently large to accommodate multiple orientations of the azabisabolene ligands, as observed in D100E and Y305F trichodiene synthase complexes reported herein (Figure 9). This comparison of multiple azabisabolene conformations and orientations provides a powerful illustration of the alternative binding modes potentially available to catalytic intermediates in cyclization cascades catalyzed by trichodiene synthase mutants in which the molecular recognition of the diphosphate is altered.

The binding of azabisabolenes to trichodiene synthase appears to be influenced by electrostatic interactions between the positively charged ammonium group of the inhibitor and the negatively charged PP_i anion. We conclude that the protein-bound conformations of these inhibitors do not mimic the productive catalytic conformation and orientation of the corresponding bisabolyl cation; instead, the azabisabolene analogues adopt thermodynamically favored conformations and orientations that correspond to catalytically nonproductive bisabolyl cation complexes. During actual catalysis, the lifetime of the bisabolyl cation is too short to allow it to adopt the most thermodynamically favored conformation and orientation. Thus, we suggest that the catalytically relevant conformation and orientation of the bisabolyl cation in the trichodiene synthase active site and possibly the conformations and orientations of other cyclization intermediates are under kinetic rather than thermodynamic control.

Intriguingly, nonproductive binding modes are also observed for the binding of two aza analogues of carbocation intermediates to bornyl diphosphate synthase (*32*). A nonproductive binding mode is also observed for the substrate analogue farnesyl hydroxyphosphonate complexed with 5-epi-aristolochene synthase (*37*, *38*). Thus, it appears to be a common theme among the greater family of the terpenoid cyclases that thermodynamically favorable binding conformations and orientations observed for certain analogues of the substrate and carbocation intermediates do not necessarily correspond to the productive binding conformations and orientations required for the analogous reaction intermediates. This observation leads to the conclusion that the formation of transient carbocation intermediates in many terpene cyclization reactions is under kinetic rather than thermodynamic control. Interestingly, however, one aza analogue of a carbocation intermediate in the formation of bornyl diphosphate, 2-azabornane, binds to bornyl diphosphate synthase in a thermodynamically favorable conformation and orientation that clearly reflects the catalytically relevant binding mode of the corresponding 2-bornyl cation just prior to its nucleophilic capture by PP_i to form bornyl diphosphate (*32*). Notably, the latter analogue is very "product-like" in structure, suggesting that for this cyclase the conformations and orientations of bound intermediates may become thermodynamically more favorable as the product structure is approached.

In summary, amino acid substitutions that alter the molecular recognition of the substrate diphosphate group in a terpene cyclase active site, such as the D100E and Y305F mutations in trichodiene synthase, lead to aberrant product formation by altering the active-site cavity and volume. Such changes alter the binding conformations of kinetically controlled and/or thermodynamically controlled intermediates, and the structures of the resultant aberrant products shed light on the structure and stereochemistry of the normally cryptic, enzyme-bound reaction intermediates. Although protein crystallographic analysis plays an increasingly indispensable role in the understanding of terpene cyclization mechanisms, a detailed understanding of mechanism and stereochemistry of the biochemical reactions themselves is essential to the proper interpretation and understanding of the wealth of information provided by protein crystallography.

ACKNOWLEDGMENT

We thank the Brookhaven National Laboratory (Beamlines X12C and X4A), the Cornell High Energy Synchrotron Source (Beamline A1), and the Advanced Light Source, Berkeley, CA (Beamline 5.0.2) for access to X-ray crystallographic data collection facilities. We thank Dr. Douglas Whittington for numerous scientific discussions.

REFERENCES

1. Buckingham, J. (1998) *Dictionary of Natural Products on CD-ROM*, version 6.1, Chapman and Hall, London, U.K.
2. Cane, D. E., Ed. (1999) *Comprehensive Natural Products Chemistry: Isoprenoids Including Carotenoids and Steroids*, Vol. 2, Elsevier, Oxford, U.K.
3. Papahadjoupoulos, D., Cowden, M., and Kimelberg, H. (1973) Role of cholesterol in membranes; effects on phospholipid−protein interactions, membrane permeability and enzymatic activity, *Biochim. Biophys. Acta 330*, 8−26.
4. McMurphie, E. J., and Raison, J. K. (1979) Membrane lipid fluidity and its effect on the activation energy of membrane-associated enzyme, *Biochim. Biophys. Acta 554*, 364−374.
5. Cane, D. E. (1985) Isoprenoid biosynthesis. Stereochemistry of the cyclization of allylic pyrophosphates, *Acc. Chem. Res. 18*, 220−226.
6. Croteau, R., and Cane, D. E. (1985) Monoterpene and sesquiterpene cyclases, *Methods in Enzymology. Steroids and Isoprenoids (Part A)*, Vol. 110, pp 383−405, Academic Press, New York.
7. Cane, D. E. (1990) Enzymatic formation of sesquiterpenes, *Chem. Rev. 90*, 1089−1103.
8. Wendt, K. U., and Schulz, G. E. (1998) Isoprenoid biosynthesis: Manifold chemistry catalyzed by similar enzymes, *Structure 6*, 127−133.
9. Lesburg, C. A., Caruthers, J. M., Paschall, C. M., and Christianson, D. W. (1998) Managing and manipulating carbocations in biology: Terpenoid cyclase structure and mechanism, *Curr. Opin. Struct. Biol. 8*, 695−703.
10. Steele, C. L., Crock, J., Bohlmann, J., and Croteau, R. (1998) Sesquiterpene synthases from Grand fir (*Abeis grandis*). Comparison of constitutive and wound-induced activities, and c-DNA isolation, characterization, and bacterial expression of δ-selinene synthase and γ-humulene synthase, *J. Biol. Chem. 273*, 2078−2089.
11. Crock, J., Wildung, M., and Croteau, R. (1997) Isolation and bacterial expression of a sesquiterpene synthase cDNA clone from peppermint (*Mentha* x *piperita*, L.) that produces the aphid alarm pheromon (*E*)-β-farnesene, *Proc. Natl. Acad. Sci. U.S.A. 94*, 12833−12838.
12. Colby, S. M., Crock, J., Dowdle-Rizzo, B., Lemaux, P. G., and Croteau, R. (1998) Germacrene C synthase from *Lycopersicon esculentum* cv. VFNT Cherry tomato: cDNA isolation, characterization, and bacterial expression of the multiple product sesquiterpene cyclase, *Proc. Natl. Acad. Sci. U.S.A. 95*, 2216−2221.
13. Mercke, P., Crock, J., Croteau, R., and Brodelius, P. E. (1999) Cloning, expression, and characterization of *epi*-cedrol synthase, a sesquiterpene cyclase from *Artemisia annua* L., *Arch. Biochem. Biophys. 369*, 213−222.

14. Mercke, P., Bengtsson, M., Bouwmeester, H. J., Posthumus, M. A., and Brodelius, P. E. (2000) Molecular cloning, expression, and characterization of amorpha-4,11-diene synthase, a key enzyme of artemisinin biosynthesis in *Artemisia annua* L., *Arch. Biochem. Biophys. 381*, 173−180.
15. He, X., and Cane, D. E. (2004) Mechanism and stereochemistry of the germacradienol/germacrene D synthase of *Streptomyces coelicolor* A3(2), *J. Am. Chem. Soc. 126*, 2678−2679.
16. Ashby, M. N., and Edwards, P. A. (1990) Elucidation of the deficiency in two yeast coenzyme Q mutants. Characterization of the structural gene encoding hexaprenyl pyrophosphate synthase, *J. Biol. Chem. 265*, 13157−13164.
17. Hohn, T. M., and Plattner, R. D. (1989) Purification and characterization of the sesquiterpene cyclase aristolochene synthase from *Penicillum roqueforti*, *Arch. Biochem. Biophys. 272*, 137−143.
18. Hohn, T. M., and vanMiddlesworth, F. (1986) Purification and characterization of the sesquiterpene cyclase trichodiene synthase from *Fusarium sporotrichiodes*, *Arch. Biochem. Biophys. 251*, 756−761.
19. Cane, D. E., Swanson, S., and Murthy, P. P. N. (1981) Trichodiene biosynthesis and the enzymatic cyclization of farnesyl pyrophosphate, *J. Am. Chem. Soc. 103*, 2136−2138.
20. Cane, D. E., Xue, Q., and Fitzsimons, B. C. (1996) Trichodiene synthase. Probing the role of the highly conserved aspartate-rich region by site-directed mutagenesis, *Biochemistry 35*, 12369−12376.
21. Rynkiewicz, M. J., Cane, D. E., and Christianson, D. W. (2001) Structure of trichodiene synthase from *Fusarium sporotrichioides* provides mechanistic inferences on the terpene cyclization cascade, *Proc. Natl. Acad. Sci. U.S.A. 98*, 13543−13548.
22. Rynkiewicz, M. J., Cane, D. E., and Christianson, D. W. (2002) X-ray crystal structures of D100E trichodiene synthase and its pyrophosphate complex reveal the basis for terpene product diversity, *Biochemistry 41*, 1732−1741.
23. Cane, D. E., Shim, J. H., Xue, Q., and Fitzsimons, B. C. (1995) Trichodiene synthase. Identification of active site residues by site-directed mutagenesis, *Biochemistry 34*, 2480−2488.
24. Cane, D. E., and Xue, Q. (1996) Trichodiene synthase. Enzymatic formation of multiple sesquiterpenes by alteration of the cyclase active site, *J. Am. Chem. Soc. 118*, 1563−1564.
25. Cane, D. E., Yang, G., Coates, R. M., Pyun, H.-J., and Hohn, T. M. (1992) Trichodiene synthase. Synergistic inhibition by inorganic pyrophosphate and aza analogs of the bisabolyl cation, *J. Org. Chem. 57*, 3454−3462.
26. Cane, D. E., Wu, Z., Oliver, J. S., and Hohn, T. M. (1993) Overproduction of soluble trichodiene synthase from *Fusarium sporotrichiodes* in *Escherichia coli*, *Arch. Biochem. Biophys. 300*, 416−422.
27. Otwinowski, Z., and Minor, W. (1997) Processing of X-ray diffraction data collected in oscillation mode, *Methods in Enzymology. Macromolecular Crystallography (Part A)*, Vol. 276, pp 307−326, Academic Press, San Diego, CA.
28. Brünger, A. T., Adams, P. D., Clore, G. M., DeLano, W. L., Gros, P., Grosse-Kunstleve, R. W., Jiang, J.-S., Kuszewski, J., Nilges, M., Pannu, N. S., Read, R. J., Rice, L. M., Simonson, T., and Warren, G. L. (1998) Crystallography and NMR system: A new software suite for macromolecular structure determination, *Acta Crystallogr., Sect. D 54*, 905−921.
29. Jones, T. A., Zou, J.-Y., Cowan, S. W., and Kjeldgaard, M. (1991) Improved methods for building protein models in electron density maps and the location of errors in these models, *Acta Crystallogr., Sect. A 47*, 110−119.
30. Bacon, D., and Anderson, W. F. (1988) A fast algorithm for rendering space-filling molecule pictures, *J. Mol. Graphics 6*, 219−220.
31. Meritt, E. A., and Murphy, M. E. P. (1994) *Raster3D* version 2.0. A program for photorealistic molecular graphics, *Acta Crystallogr., Sect. D 50*, 869−873.
32. Whittington, D. A., Wise, M. L., Urbansky M, Coates, R. M., Croteau, R. B., and Christianson, D. W. (2002) Bornyl diphosphate synthase: Structure and strategy for carbocation manipulation by a terpenoid cyclase, *Proc. Natl. Acad. Sci. U.S.A. 99*, 15375−15380.
33. Liang, J., Edelsbrunner, H., and Woodward, C. (1998) Anatomy of protein pockets and cavities: Measurement of binding site geometry and implications for ligand design, *Protein Sci. 7*, 1884−1897.
34. Liang, J., Edelsbrunner, H., Fu, P., Sudhakar, P. V., and Subramaniam, S. (1998) Analytical shape computation of macromolecules: II. Inaccessible cavities in proteins, *Proteins 33*, 18−29.
35. Liang, J., Edelsbrunner, H., Fu, P., Sudhakar, P. V., and Subramaniam, S. (1998) Analytical shape computation of macromolecules: I. Molecular area and volume through α shape, *Proteins 33*, 1−17.
36. Cane, D. E., Chiu, H.-T., Liang, P.-H., and Anderson, K. S. (1997) Pre-steady-state kinetic analysis of the trichodiene synthase reaction pathway, *Biochemistry 36*, 8332−8339.
37. Starks, C. M., Back, K., Chappell, J., and Noel, J. P. (1997) Structural basis for cyclic terpene biosynthesis by tobacco 5-epi-aristolochene synthase, *Science 277*, 1815−1820.
38. Rising, K. A., Starks, C. M., Noel, J. P., and Chappell, J. (2000) Demonstration of germacrene A as an intermediate in 5-epi-aristolochene synthase catalysis, *J. Am. Chem. Soc. 122*, 1861−1866.
39. Kleywegt, G. J., and Jones, T. A. (1993) Biomacromolecular speleology, *ESF/CCP4 Newsl. 29*, 26−28.
40. Kleywegt, G. J., and Jones, T. A. (1994) Detection, delineation, measurement and display of cavities in macromolecular structures, *Acta Crystallogr., Sect. D 50*, 178−185.

BI050059O